Universal time delays in the inelastic core level photoemission of metals

Gimin Bae,* Hyosub Park,* and J. D. Lee†
Department of Emerging Materials Science, DGIST, Daegu 42988, Republic of Korea

(Received 3 November 2020; revised 31 March 2021; accepted 1 April 2021; published 14 April 2021)

Proposing a theoretical model of the core level photoemission of metals, we investigate the plasmon-driven inelastic photoemission delays based on a nonperturbative treatment of many-electron responses due to the long-range Coulomb potential. Being irrelevant to the plasmon coupling strength as well as the plasmon frequency, the emission delays $\Delta\tau_n$ of the nth-order plasmon satellites ($n = 1, 2, 3, \ldots$) are found to be universal order by order among the metals in the core level photoemission where the recoil-less approximation would be valid. In particular, for a main line with its weight $e^{-\gamma}$, where γ quantifies the plasmon coupling strength, the average inelastic photoemission delay $\langle\Delta\tau\rangle$ is found to be $\gamma(1-e^{-\gamma})^{-1}\Delta\tau_1$ and thus is simply scaled by a universal time delay $\Delta\tau_1$. This finding is sharply contrasted with the emission delays under the localized potential, which indicates a fundamental difference in the emission process between extended and localized screenings.

DOI: 10.1103/PhysRevB.103.165413

I. INTRODUCTION

Single attosecond (1 as $= 10^{-18}$ s) pulses in the extreme ultraviolet (XUV) frequency range allow time-domain insight into fundamental electronic processes in atoms, molecules, and solids at the timescale of 10–100 as [1–18]. Photoemission spectroscopy stemming from Einstein's photoelectric effect is an ideal target of such investigation. Conventionally, the photoemission spectroscopy simply analyzes the kinetic energy distribution of photoemitted electrons for a given continuous wave light source. A novel form of the attosecond photoemission with a combination of attosecond XUV pulse and synchronized femtosecond (1 fs $= 10^{-15}$ s) infrared (IR) pulse has opened a new chapter to the time-domain understanding of the first stage of photoemission processes such as photoexcitation and transport [1–3,5,7].

A photoelectron emitted by the attosecond XUV pulse could be streaked by the femtosecond IR pulse with a variable relative delay. The first proof of the principle experiment has shown a time delay of about 100 as (100 ± 70 as) between photoelectrons from the $4f$ core level and the conduction band of tungsten metal [2]. Subsequently, for the atomic target of neon, the $2s$ electron was found to be emitted earlier than the $2p$ electron by 21 ± 5 as [3] and the electron-electron correlation was also studied in the photoionization [4]. Similarly, for the atomic argon, the emission of $3s$ and $3p$ electrons was examined [5]. For the van der Waals crystal tungsten diselenide (WSe_2), the emission delay has been investigated by accounting for the ionization and transport delays [6]. In a magnesium surface [i.e., Mg(0001) surface], the photoelectron was found to be launched simultaneously from the localized core level and the delocalized valence-band state [7] and later the inelastic photoemission delay due to the extrinsic plasmon loss was also resolved [8]. Recently, attosecond dynamics of the valence-band photoexcitation on the magnesium surface have been studied [9,10].

Photoelectron emission delay of solids would be described by the ionization delay occurring in the intra-atomic potential scattering [i.e., the Eisenbud-Wigner-Smith (EWS) delay] [19] and the transport delay in the propagation to the surface. The transport delay may be again considered in two respects: One is the delay of the drifting electron under the crystal potential and the other is the inelastic delay due to the extrinsic loss of photoelectrons. In the theoretical respect, the former is handled by exploring the propagation of the photoelectron wave function $\Psi(z,\tau)$ from a solution of the one-dimensional Schrödinger equation under the one-particle crystal potential [20]; however the latter is a challenge because it is under the many-body potential. A proper approach to the inelastic delay caused by the extrinsic loss of solids is still lacking.

In this paper, we propose a theoretical model to describe the inelastic photoemission delay driven by the extrinsic plasmon loss in the core level photoemission of a metallic electron system. By solving the many-body time-dependent Schrödinger equation, we calculate the photoemission spectra up to the first-order plasmon satellite including the extrinsic loss. This could be extrapolated to the infinite-order spectra based on an idea of the cumulant expansion of the nonperturbative theory. The cumulant expansion will be exact in the limit of the zero bandwidth corresponding to a dispersionless core level, i.e., in the limit that the recoil-less approximation would be generally valid. The emission delay $\Delta\tau_1$ of the first-order plasmon satellite is found to be universal among the metals in that it is irrelevant to the plasmon frequency and the plasmon coupling strength. At the same time, emissions of higher-order plasmon satellites are found to be delayed by $2\Delta\tau_1$, $3\Delta\tau_1$, and so on, and universal as well. Furthermore, when the weight of the main line is $e^{-\gamma}$, the average inelastic delay $\langle\Delta\tau\rangle$ is given by $\gamma(1-e^{-\gamma})^{-1}\Delta\tau_1$ and scaled by a

*These authors contributed equally to this work.
†jdlee@dgist.ac.kr

universal delay $\Delta\tau_1$ up to a constant. γ quantifies the plasmon coupling strength. Our finding is definitely different from the emission delay in localized systems, which is eventually traced to the fundamental difference in the photohole screening between extended and localized systems.

The paper is organized as follows. In Sec. II, we introduce a model Hamiltonian of the core level photoemission of metals and a theoretical formulation for the nonperturbative treatment. In Sec. III, we provide the photoelectron emission delays for inelastic plasmon satellites and point out a universal time delay. We also discuss the origin of the universality. In Sec. IV, we give a Summary and Conclusion.

II. MODEL AND THEORETICAL FORMULATION

During the photoemission of core level electrons, the inelastic satellites develop by exciting plasmon $\omega_{\mathbf{q}}$ from the fluctuating conduction electrons in the Fermi sea. A model Hamiltonian $\mathcal{H}$ describing the relevant physical process can be written as

$$\mathcal{H} = \varepsilon_c c^\dagger c + \sum_{\mathbf{q}} \omega_{\mathbf{q}} a_{\mathbf{q}}^\dagger a_{\mathbf{q}} + A_{\mathrm{XUV}}(\tau) \sum_{\mathbf{k}} (c_{\mathbf{k}}^\dagger c + c^\dagger c_{\mathbf{k}}) + \sum_{\mathbf{q}} V_{\mathbf{q}}^c c^\dagger c (a_{-\mathbf{q}} + a_{\mathbf{q}}^\dagger) + \sum_{\mathbf{k}} [\varepsilon_{\mathbf{k}} - \mathbf{k}\cdot\mathbf{A}_{\mathrm{IR}}(\tau + \tau_{\mathrm{IR-XUV}})] c_{\mathbf{k}}^\dagger c_{\mathbf{k}} + \sum_{\mathbf{kq}} V_{\mathbf{k},\,\mathbf{k+q}} c_{\mathbf{k}}^\dagger c_{\mathbf{k+q}} (a_{-\mathbf{q}} + a_{\mathbf{q}}^\dagger). \tag{1}$$

$\mathcal{H}$ includes the photoelectron excitation by the XUV pulse, the concomitant shaking of conduction electrons (i.e., exciting plasmon), the photoelectron streaking by the IR pulse, and the photoelectron scattering with plasmons, which is attributed to the extrinsic loss. In Eq. (1), $c^\dagger$ (or c), $c_{\mathbf{k}}^\dagger$ (or $c_{\mathbf{k}}$), and $a_{\mathbf{q}}^\dagger$ (or $a_{\mathbf{q}}$) imply the operators of core level electron, photoelectron, and bulk plasmon with their energies ε_c, $\varepsilon_{\mathbf{k}} = \frac{1}{2}\mathbf{k}^2$, and $\omega_{\mathbf{q}} = \omega_{\mathrm{pl}} + \frac{1}{2}\mathbf{q}^2$, respectively. For a simple fluctuation potential $V_{\mathbf{q}}(\mathbf{r}) = V_{\mathbf{q}}^0 e^{-i\mathbf{q}\cdot\mathbf{r}}$ due to the plasmon excitation, $V_{\mathbf{q}}^c$ is given by $V_{\mathbf{q}}(\mathbf{r}_c)$, where $\mathbf{r}_c$ is the position of the core hole, and the matrix element $V_{\mathbf{k},\,\mathbf{k+q}}$ is reduced to $\langle\mathbf{k}|V_{\mathbf{q}}|\mathbf{k}+\mathbf{q}\rangle = V_{\mathbf{q}}^0$. Here the plasmon coupling strength $V_{\mathbf{q}}^0$ is $\xi\sqrt{4\pi\omega_{\mathrm{pl}}^2/V\mathbf{q}^2\omega_{\mathbf{q}}}$ [21], i.e., originally due to the long-range Coulomb potential. ξ will be used as a parameter to control the potential strength.

For the parameters, we assume $\varepsilon_c = -50$ eV for the magnesium $2p$ core level and $\omega_{\mathrm{pl}} = 10.6$ eV for the density of metallic electrons of magnesium. $\mathbf{A}_{\mathrm{XUV}}(\tau)$ is the photoexciting attosecond XUV pulse given by $\mathbf{A}_{\mathrm{XUV}}(\tau) = A_{\mathrm{XUV}} \exp[-\tau^2/\bar{\tau}_{\mathrm{XUV}}^2]\cos(\omega_{\mathrm{XUV}}\tau)\hat{\mathbf{e}}_{\mathrm{XUV}}$ and $\mathbf{A}_{\mathrm{IR}}(\tau)$ is the probing femtosecond IR pulse given by $\mathbf{A}_{\mathrm{IR}}(\tau) = A_{\mathrm{IR}} \exp[-\tau^2/\bar{\tau}_{\mathrm{IR}}^2]\cos(\omega_{\mathrm{IR}}\tau)\hat{\mathbf{e}}_{\mathrm{IR}}$. $\omega_{\mathrm{IR}} = 1.63$ eV is taken. XUV and IR pulses are assumed to be linearly polarized along the photoelectron detection. Half widths at half maxima (HWHMs) of the two pulses are now 165.6 as and 2.5 fs. $\tau_{\mathrm{IR-XUV}}$ is a controllable relative delay of the IR pulse from the XUV pulse.

Up to the first-order ($n = 1$) plasmon satellite, the photoemission process is described by the quantum state $|\Psi(\tau)\rangle$ in the limit of $A_{\mathrm{XUV}} \to 0$,

$$|\Psi(\tau)\rangle = C(\tau)|c\rangle|0'\rangle + \sum_{\mathbf{k}} C_{\mathbf{k}}(\tau)|\mathbf{k}\rangle|0\rangle + \sum_{\mathbf{k}}\sum_{\mathbf{q}} C_{\mathbf{kq}}(\tau)|\mathbf{k}\rangle|\mathbf{q}\rangle, \tag{2}$$

where $|c\rangle$ and $|\mathbf{k}\rangle$ stand for the states of core level electron and photoelectron, $|0'\rangle$ $(= e^{-\sum_{\mathbf{q}} \frac{V_{\mathbf{q}}^c}{\omega_{\mathbf{q}}} a_{\mathbf{q}}^\dagger}|0\rangle \approx [1 - \sum_{\mathbf{q}} \frac{V_{\mathbf{q}}^c}{\omega_{\mathbf{q}}} a_{\mathbf{q}}^\dagger]|0\rangle)$ is the vacuum state without a core hole, and $|0\rangle$ and $|\mathbf{q}\rangle$ are the states of vacuum and plasmon with a core hole. By solving the time-dependent Schrödinger equation $i\hbar\partial/\partial\tau|\Psi(\tau)\rangle = \mathcal{H}|\Psi(\tau)\rangle$ with an initial condition of $|\Psi(\tau_0)\rangle = |c\rangle|0'\rangle$ at $\tau = \tau_0$ ($\tau_0 \ll -\bar{\tau}_{\mathrm{XUV}}$), we could calculate the photoemission spectrum $J(\omega,\ \tau_{\mathrm{IR-XUV}}) = |C_{\mathbf{k}}(\tau_{\max})|^2 + \sum_{\mathbf{q}} |C_{\mathbf{kq}}(\tau_{\max})|^2$ with $\omega = \mathbf{k}^2/2$ at a given value of $\tau_{\mathrm{IR-XUV}}$. $|C_{\mathbf{k}}(\tau_{\max})|^2$ and $\sum_{\mathbf{q}} |C_{\mathbf{kq}}(\tau_{\max})|^2$ make the main line and the $n = 1$ plasmon satellite, respectively. $\tau_{\max}$ is the time at which the spectrum is fully converged. The last term of Eq. (1) leads to the extrinsic plasmon loss and drives the inelastic photoemission delay as will be shown later. Without it, the plasmon satellite simply reduces to the intrinsic one. In Fig. 1(a), through R and α, relative weights of the main line and the (intrinsic and/or extrinsic) satellite are illustrated.

Through a cumulant expansion [22], a partial summation of the contributions of $V_{\mathbf{q}}$ in the first-order perturbation theory could be extrapolated to the infinite-order spectra $P(\omega)$,

$$P(\omega) = \int \frac{d\tau}{2\pi} e^{-i\omega\tau} \exp\left[\int d\omega' \beta(\omega') \frac{e^{i\omega'\tau} - 1}{\omega'}\right], \tag{3}$$

where $\beta(\omega)/\omega$ should correspond to $\sum_{\mathbf{q}} |C_{\mathbf{kq}}(\tau_{\max})|^2$. An integral in the exponent of Eq. (3) is well defined for small ω' and finite τ, but we may have trouble with its numerical treatment in the limit of $\omega' = 0$ for large τ. Therefore, we will not try a direct calculation of $P(\omega)$ and instead convert to an integral equation. We then have

$$\omega P(\omega) = \int_0^\omega d\omega' \beta(\omega') P(\omega - \omega'),$$

which will be actually used for an evaluation of Eq. (3). According to previous studies, the lowest-order core-induced plasmon emission generates a cumulant representation of the spectrum [23], likewise the emission by photoexcited valence-/conduction-band electrons [24]. However, as a rule the interference processes involving the interplay between the core hole and photoexcited electron coupling to plasmons do not [25,26], unless the electron motion can be treated in the recoil-less regime [27]. In Fig. 1(b), a diagrammatic expansion to the infinite-order spectra $P(\omega)$ from $\beta(\omega)$, i.e., corresponding to the cumulant expansion, is schematically

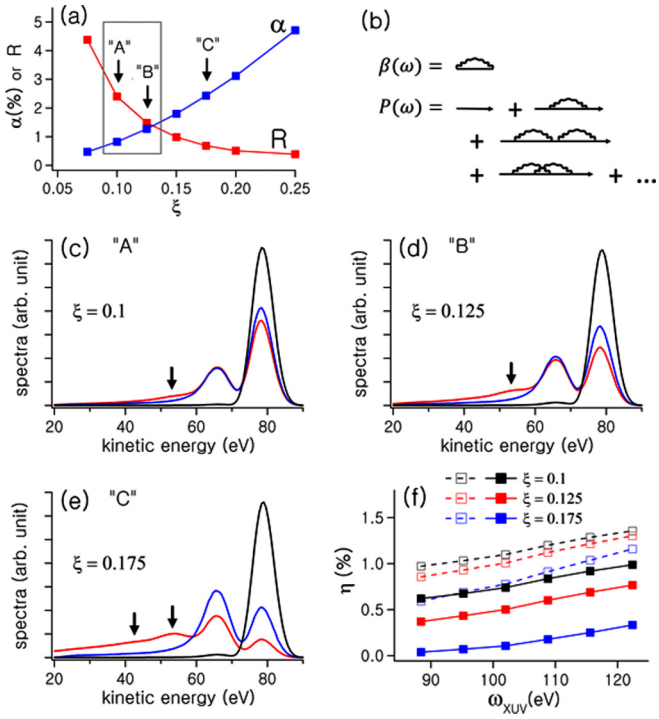

FIG. 1. Nonperturbative treatment of core level photoemission of metal. (a) R and α with respect to ξ. R and α are defined by $R = I_{\rm main}/[I^{\rm intr}_{n=1} + I^{\rm extr}_{n=1}]$ and $\alpha = I^{\rm intr}_{n=1}/[I_{\rm main} + I^{\rm intr}_{n=1}]$, where $I_{\rm main}$ denotes the spectral weight of the main line and $I^{\rm intr}_n$ or $I^{\rm extr}_n$ the intrinsic or extrinsic satellites up to the nth order. The gray box may accord roughly with the case of magnesium $2p$ plasmon lines [8]. (b) Extrapolation to the infinite-order spectra $P(\omega)$ from $\beta(\omega)$ in terms of the diagrammatic expansion. Solid lines denote electron and wavy lines plasmon. (c)–(e) $J_0(\omega)$ (black line), $J(\omega)$ (blue line), and $P(\omega)$ (red line) for values of $\xi = 0.1$, 0.125, and 0.175, respectively. Arrows indicate higher-order plasmon satellites. All the spectra are evaluated at $\tau_{\rm IR-XUV} = 0$ and normalized by their area. (f) $\eta = I^{\rm intr}_n/I^{\rm extr}_n$ with respect to ξ. Empty squares are for $n = 1$ and filled squares for $n = \infty$.

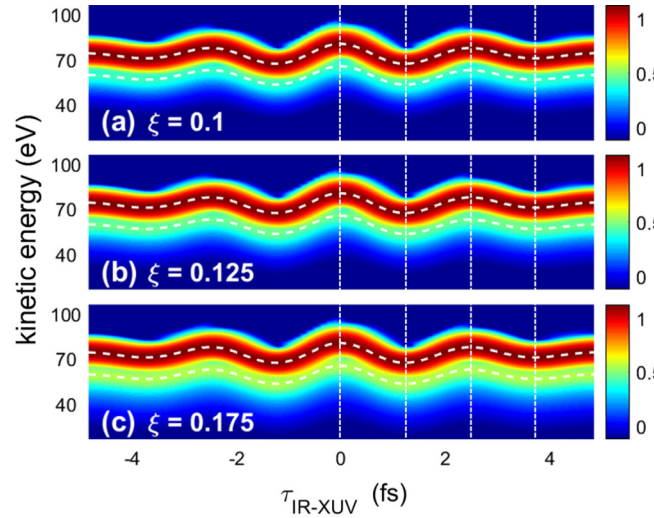

FIG. 2. Spectrogram of intrinsic $n = 1$ photoemission. (a)–(c) Centers of gravity (white dashed lines) of two features (i.e., main and intrinsic satellite) of the intrinsic photoemission spectra $J_0(\omega)$ with respect to $\tau_{\rm IR-XUV}$ for values of $\xi = 0.1$, 0.125, and 0.175. Vertical (white dashed) lines are simply guides to the eye.

illustrated. It should be noted that a summation of diagrams does not include a bubble one, which implies that the cumulant expansion will be exact in the vanishing bandwidth, for instance, a perfectly dispersionless level or a very deep core level (probably consistent with our consideration of the magnesium $2p$ core level with $\varepsilon_c = -50$ eV). Furthermore, the expansion would be expected to be valid within the recoil-less approximation neglecting recoil momenta of electrons and holes by excited plasmons. Figures 1(c)–1(e) provide the intrinsic $n = 1$ spectra $J_0(\omega)$, the $n = 1$ spectra $J(\omega)$, and the infinite-order spectra $P(\omega)$ for $\xi = 0.1$, 0.125, and 0.175 at $\tau_{\rm IR-XUV} = 0$. It is noted that $J(\omega)$ and $P(\omega)$ include both intrinsic and extrinsic losses. In the figures, higher-order ($n = 2$ or $n = 3$) plasmon satellites are clearly seen in $P(\omega)$ (as indicated by arrows). In Fig. 1(f), weight ratios of intrinsic and extrinsic satellites are given for selected ξ's.

III. RESULTS AND DISCUSSION

In Fig. 2, spectrograms of $J_0(\omega)$ are displayed with respect to $\tau_{\rm IR-XUV}$ for a few values of ξ. In the figure, the emission delay $\Delta\tau$ between the main and intrinsic plasmon satellite is estimated to be less than 2 as, which may in fact conclude that $\Delta\tau = 0$ within the numerical accuracy. An estimation of $\Delta\tau$ is done in the present study by fitting the spectrograms using the eighth-order Fourier series. In contrast, in spectrograms of $P(\omega)$ (see Fig. 3), systematic nonzero delays of plasmon satellites relative to the main line are observed depending on $\omega_{\rm XUV}$. Moreover, the $n = 2$ plasmon satellite (white dashed lines) is found further delayed from the $n = 1$ plasmon satellite. From a comparison with the intrinsic photoemission, it is critical to note that our model properly captures the relative transport delays due to the inelastic photoelectron scattering, where the EWS delays would not be relevant because they are contained in all the satellites including the main line.

Figures 4(a) and 4(b) deliver the inelastic photoemission delays $\Delta\tau_1$, $\Delta\tau_2$, and $\Delta\tau_3$ of $n = 1, 2$, and 3 plasmon satellites with respect to the photoelectron kinetic energy (i.e., depending on $\omega_{\rm XUV}$) for various potential strengths ξ and plasmon frequencies $\omega_{\rm pl}$, respectively. In the figures, it is remarkable to find that the emission delays $\Delta\tau_n$ of the nth-order plasmon satellites would be universal among the metals in that they hardly depend on the plasmon potential strength as well as the plasmon frequency. Furthermore, $\Delta\tau_n$ is found to be approximately n times as long as $\Delta\tau_1$,

$$\Delta\tau_1 \sim \lambda/v,$$

where v is given by $\sqrt{2\varepsilon}$ and λ is an average distance propagated by the photoelectron without any inelastic scattering. The photoelectron suffering two consecutive inelastic scatterings gets to be doubly delayed compared to the photoelectron scattered once and, that is, higher-order plasmon satellites would then be delayed as $2\Delta\tau_1$, $3\Delta\tau_1$, and so on. Equation (3) can now be expressed as follows, by making an expansion

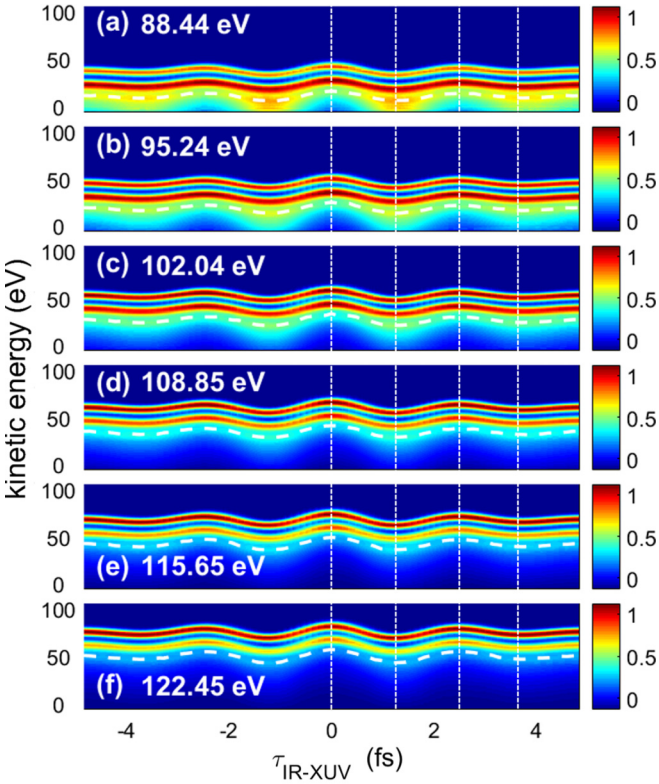

FIG. 3. Spectrogram of infinite-order photoemission. (a)–(f) Spectrograms of three features (i.e., main, $n = 1$ satellite, and $n = 2$ satellite) of $P(\omega)$ with respect to τ_{IR-XUV} for values of $\omega_{XUV} = 88.44$, 95.24, 102.04, 108.85, 115.65, and 122.45 eV at a fixed value of $\xi = 0.125$. Centers of gravity of the $n = 2$ satellite features are given in white dashed lines. Meanwhile, it is a typical observation that the extrinsic plasmon losses are strengthened as ω_{XUV} decreases. Vertical (white dashed) lines are simply guides to the eye.

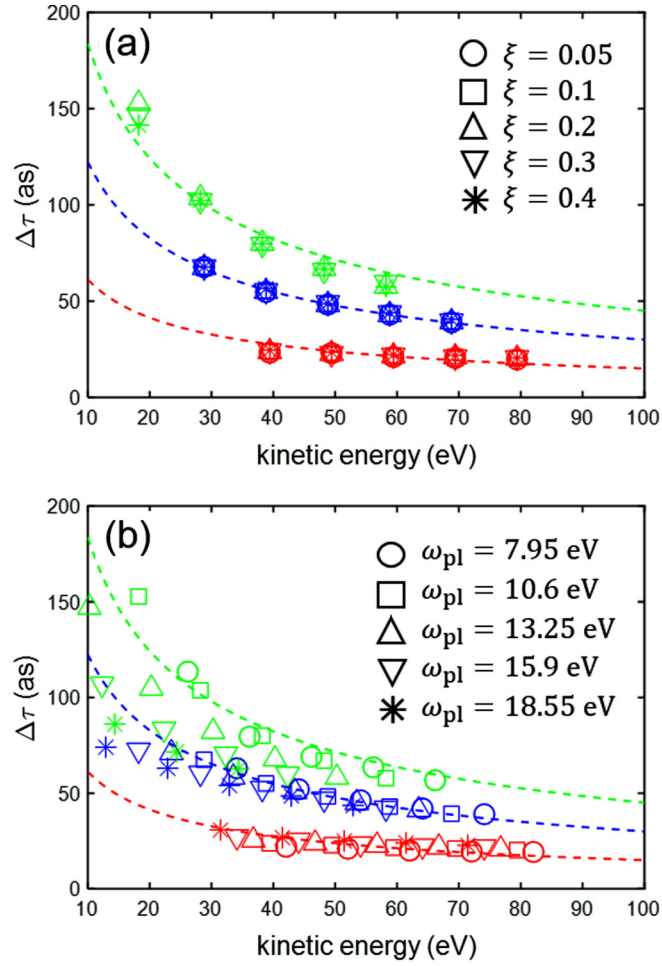

FIG. 4. Delay of inelastic photoelectron emission. (a) Photoemission delays $\Delta\tau_1$, $\Delta\tau_2$, and $\Delta\tau_3$ of $n = 1$ (red), $n = 2$ (blue), and $n = 3$ (green) satellites relative to the main line with respect to the photoelectron kinetic energy for values of ξ. $\omega_{pl} = 10.6$ eV is adopted. Red dashed curve fits to $\Delta\tau_1$. Blue dashed curve doubles and green dashed curve triples the red dashed one. (b) Photoemission delays for values of ω_{pl}. $\xi = 0.2$ is adopted. In the calculation, HWHM of the XUV pulse is taken to be 331 as.

of the integrand,

$$P_{sat}(\omega) = e^{-\gamma}\left[\frac{\beta(\omega)}{\omega} + \frac{1}{2}\int d\omega' \frac{\beta(\omega')\beta(\omega-\omega')}{\omega'(\omega-\omega')} + \ldots\right],$$

where $P_{sat}(\omega)$ is the satellite spectra, i.e, $P_{sat}(\omega) = P(\omega) - e^{-\gamma}\delta(\omega)$, and γ is given by $\gamma = \int d\omega'\beta(\omega')/\omega'$. If one integrates $P_{sat}(\omega)$ term by term, one can obtain the spectral weight of each order plasmon satellite obeying the Poisson stochastic distribution as $\int d\omega P_{sat}(\omega) = e^{-\gamma}[\gamma + \frac{1}{2}\gamma^2 + \ldots]$. Then an average inelastic photoemission delay $\langle\Delta\tau\rangle$ is given by

$$\langle\Delta\tau\rangle = \frac{\sum_{n=1}^{\infty}\frac{\Delta\tau_n\gamma^n}{n!}}{\sum_{n=1}^{\infty}\frac{\gamma^n}{n!}} = \gamma(1-e^{-\gamma})^{-1}\Delta\tau_1,$$

and found to be simply scaled by a universal delay $\Delta\tau_1$ up to a constant. $\langle\Delta\tau\rangle$ simply gets to be $\Delta\tau_1$ in a limit of $\gamma \ll 1$. This strongly suggests a universal curve of the electron mean free path of metals [28] from a microscopic point of view of the photoemission delay. Simultaneously, this is unquestionably distinguished from localized systems, for instance, atoms, molecules, insulating solids, and so on.

In a localized electronic environment, the photoelectron passes through a short-range attractive potential made out of an efficient screening of the photohole and attains a negative delay (i.e., the EWS delay) compared to the free space [29]. The negative delay may be qualitatively understood by an increase of the electron velocity in the potential range. The situation would be readily understood from a simple one-dimensional classical model of the photoelectron on a trajectory, i.e., $\rho(z,\tau) = \delta(z + v\tau - z_c)$ at $\tau > 0$. $v\ (= \sqrt{2\varepsilon})$ is the velocity of the photoelectron and z_c the position of the core hole. Taking the localized potential given by $V(z) = V_0\zeta(z)$ [see Fig. 5(a)], the time-dependent scattering potential $V(\tau)$ is obtained as $V(\tau) = \int dz V(z)\rho(z,\tau)$. From the first-order time-dependent perturbation theory, the transition amplitude M is evaluated to be $M = 1 - i\int_0^\infty d\tau V(\tau) = 1 - i\frac{V_0}{v}D$, where D is an effective range of the potential. The phase shift $\delta(\varepsilon)$ is given by $\delta(\varepsilon) = \tan^{-1}[\mathrm{Im}M/\mathrm{Re}M] = -\tan^{-1}[V_0 D/v]$ and the emission delay $\Delta\tau$ will then be $\partial\delta(\varepsilon)/\partial\varepsilon$. Here, the delay directly depends on the depth and width of the scattering potential. In contrast, a screening of the photohole by the

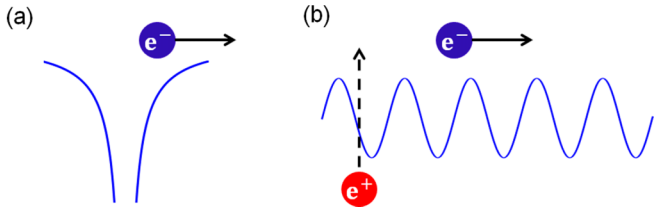

FIG. 5. Schematics of photoelectron scattering. (a) Photoemission under the localized attractive potential. A photohole is well screened by local states. (b) Photoemission under the extended plasmon potential (i.e., outside the intra-atomic sector of metal). A photohole is not well screened by extended states.

extended states in a metallic environment would not be so efficient [30]. In that case, therefore, the one-dimensional classical model of the photoelectron, simultaneously with the photohole, i.e., $\rho(z,\tau) = [\delta(z + v\tau - z_c) - \delta(z - z_c)]$ at $\tau > 0$ [21], would be available. Assuming the plasmon-induced fluctuation potential $V_q(z)$ $(= V_q^0 e^{iqz})$, the photoelectron-plasmon scattering potential $V_q(\tau)$ is obtained as $V_q(\tau) = \int dz\, V_q(z)\rho(z,\tau)$ [see Fig. 5(b)]. For a proper calculation of the time-dependent perturbation, we choose to gradually turn off the perturbation potential as $V_q(\tau) \to e^{-\eta\tau}V_q(\tau)$ with $\eta > 0$. From the first-order time-dependent perturbation theory, the q-dependent transition amplitude M_q is evaluated to be $M_q = -i\int_0^\infty d\tau e^{i\omega_q\tau}e^{-\eta\tau}V_q(\tau)$. The q-dependent phase shift $\delta_q(\varepsilon)$ is $\delta_q(\varepsilon) = \tan^{-1}[\mathrm{Im}M_q/\mathrm{Re}M_q]$, which is clearly irrelevant to the scattering potential strength V_q^0. The q-dependent emission delay $\Delta\tau_1(q)[= \frac{\partial\delta_q(\varepsilon)}{\partial\varepsilon}]$ should be likewise. Eventually, the emission delay $\Delta\tau_1$ may then be defined as a simple average, i.e., $\Delta\tau_1 = \frac{1}{N}\sum_q \Delta\tau_1(q)$. Similar arguments would be applied to the higher-order perturbation theory. A pure quantum mechanical approach will also lead to the same conclusion [21,30]. Details on the classical model of the photoelectron on a trajectory are discussed in the Appendix.

IV. SUMMARY AND CONCLUSION

To summarize, we theoretically examined the plasmon-driven inelastic photoemission delay in the core level photoemission of metals using a scheme of the nonperturbative expansion. Solving the many-body time-dependent Schrödinger equation, we obtained the main line and the first-order plasmon satellite containing the extrinsic loss, which was extrapolated to the infinite-order spectra. The extrapolation would be feasible within the recoil-less approximation usually applied to the flat core level. We then found that the emission delays $\Delta\tau_n$ of the nth-order plasmon satellites are universal order by order irrespective of metal-specific characteristics in that they are irrelevant to the plasmon scattering strength and the plasmon frequency. Furthermore, the average inelastic photoemission delay $\langle\Delta\tau\rangle$ is found to be simply scaled by a universal time delay $\Delta\tau_1$. This strongly suggests a universal curve of the electron mean free path of metals from a viewpoint of the photoemission delay. Noting that the present finding is in striking contrast with the emission delay under the localized potential, we indicate a fundamental difference in the photoelectron scattering between extended and localized screenings.

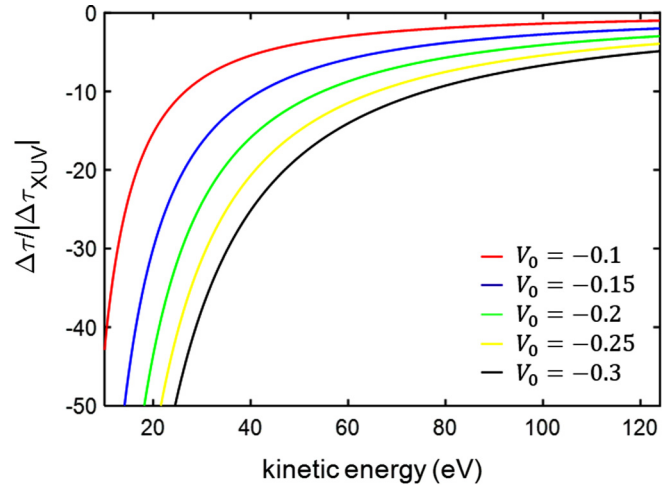

FIG. 6. Photoelectron emission delay in one-dimensional semiclassical model of the localized scattering potential for various values of V_0. A width D of the potential is adopted to be 1. $\Delta\tau_{XUV}$ is the delay calculated at the photoelectron kinetic energy of 124 eV, i.e., the upper energy bound of the extreme ultraviolet (XUV) radiation range, with $V_0 = -0.1$. A unit of V_0 and D is the atomic unit.

ACKNOWLEDGMENTS

This work was supported by the Basic Science Research Program (2019R1A2C1005050) through the National Research Foundation of Korea (NRF) and also by the DGIST R&D Programs (21-CoE-NT-01), funded by the Ministry of Science and ICT.

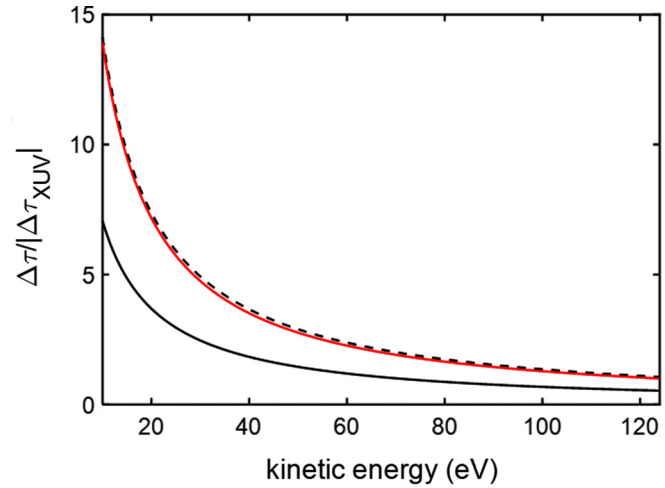

FIG. 7. Photoelectron emission delay in one-dimensional semiclassical model of the extended plasmon scattering potential. First-order (black) and second-order (red) photoemission delays are given. The black dashed line indicates twice the first-order delay. $\Delta\tau_{XUV}$ is the delay calculated at the photoelectron kinetic energy of 124 eV.

APPENDIX: DIFFERENCE IN THE EMISSION PROCESS BETWEEN LOCALIZED AND METALLIC SYSTEMS

1. Localized system

In Fig. 6, the photoelectron in a one-dimensional localized potential is shown to have negative emission delays as is well known. The delay is demonstrated to depend on the depth and width of the scattering potential.

2. Metallic system

The first-order photoelectron phase shift is given by

$$\delta_q^{(1)}(\varepsilon) = \tan^{-1}\left[-\eta\left(\frac{1}{\omega_q} + \frac{1}{\omega_q - qv}\right)\right],$$

and the emission delay is obtained by taking the derivative of $\delta_q^{(1)}(\varepsilon)$ with respect to ε $(= v^2/2)$. From the boundary condition that the photoelectron is emitted to a semi-infinite space with $z < 0$, we choose to take $q < 0$. The second-order transition amplitude is

$$M^{(2)}_{q_1,q_2}(\varepsilon) = -\frac{1}{2!}\int_0^\infty d\tau_1 e^{i\omega_{q_1}\tau_1 - \eta\tau_1} V_{q_1}(\tau_1) \times \int_0^{\tau_1} d\tau_2 e^{i\omega_{q_2}\tau_2 - \eta\tau_2} V_{q_2}(\tau_2),$$

and is evaluated to be

$$M^{(2)}_{q_1,q_2}(\varepsilon) = \frac{V^0_{q_1}V^0_{q_2}}{2}\frac{1}{i\omega_{q_1} - \eta}\frac{iq_2 v}{i(\omega_{q_1} + \omega_{q_2} - q_2 v) - 2\eta}\frac{1}{i(\omega_{q_1} + \omega_{q_2}) - 2\eta} - \frac{V^0_{q_1}V^0_{q_2}}{2}\frac{1}{i(\omega_{q_1} - q_1 v) - \eta}\frac{iq_2 v}{i(\omega_{q_1} + \omega_{q_2} - q_1 v - q_2 v) - 2\eta}\frac{1}{i(\omega_{q_1} + \omega_{q_2} - q_1 v) - 2\eta}.$$

The corresponding phase shift is then given by

$$\delta^{(2)}_{q_1,\,q_2}(\varepsilon) = \tan^{-1}\frac{\mathrm{Im}\left[M^{(2)}_{q_1,q_2}(\varepsilon)\right]}{\mathrm{Re}\left[M^{(2)}_{q_1,q_2}(\varepsilon)\right]}.$$

The second-order delay $\Delta\tau_2$ is evaluated from $\Delta\tau_2 = \frac{1}{N^2}\sum_{q_1,q_2}\tau^{(2)}_{q_1,\,q_2}(\varepsilon)$. In Fig. 7, the photoelectron emission delays are qualitatively consistent with Fig. 4 of the main text and do not depend on the potential strength. In particular, the second-order delay $\Delta\tau_2$ is found to be $\approx 2\Delta\tau_1$, which is also consistent with Fig. 4 of the main text, i.e., the nonperturbative treatment of the time-dependent Schrödinger equation. Here it is found that the emission delay in the metallic screening tends to decrease more slowly with respect to the photoelectron kinetic energy compared to the localized screening. This is actually compatible with a general understanding.

[1] F. Krausz and M. Ivanov, Attosecond physics, Rev. Mod. Phys. **81**, 163 (2009).

[2] A. L. Cavalieri, N. Müller, Th. Uphues, V. S. Yakovlev, A. Baltuška, B. Horvath, B. Schmidt, L. Blümel, R. Holzwarth, S. Hendel, M. Drescher, U. Kleineberg, P. M. Echenique, R. Kienberger, F. Krausz, and U. Heinzmann, Attosecond spectroscopy in condensed matter, Nature **449**, 1029 (2007).

[3] M. Schultze, M. Fieß, N. Karpowicz, J. Gagnon, M. Korbman, M. Hofstetter, S. Neppl, A. L. Cavalieri, Y. Komninos, T. Mercouris, C. A. Nicolaides, R. Pazourek, S. Nagele, J. Feist, J. Burgdörfer, A. M. Azzeer, R. Ernstorfer, R. Kienberger, U. Kleineberg, E. Goulielmakis *et al.*, Delay in photoemission, Science **328**, 1658 (2010).

[4] J. J. Omiste and L. B. Madsen, Attosecond photoionization dynamics in neon, Phys. Rev. A **97**, 013422 (2018).

[5] K. Klünder, J. M. Dahlström, M. Gisselbrecht, T. Fordell, M. Swoboda, D. Guénot, P. Johnsson, J. Caillat, J. Mauritsson, A. Maquet, R. Taïeb, and A. L'Huillier, Probing Single-Photon Ionization on the Attosecond Time Scale, Phys. Rev. Lett. **106**, 143002 (2011).

[6] F. Siek, S. Neb, P. Bartz, M. Hensen, C. Strüber, S. Fiechter, M. Torrent-Sucarrat, V. M. Silkin, E. E. Krasovskii, N. M. Kabachnik, S. Fritzsche, R. D. Muiño, P. M. Echenique, A. K. Kazansky, N. Müller, W. Pfeiffer, and U. Heinzmann, Angular momentum-induced delays in solid-state photoemission enhanced by intra-atomic interactions, Science **357**, 1274 (2017).

[7] S. Neppl, R. Ernstorfer, E. M. Bothschafter, A. L. Cavalieri, D. Menzel, J. V. Barth, F. Krausz, R. Kienberger, and P. Feulner, Attosecond Time-Resolved Photoemission from Core and Valence States of Magnesium, Phys. Rev. Lett. **109**, 087401 (2012).

[8] C. Lemell, S. Neppl, G. Wachter, K. Tőkési, R. Ernstorfer, P. Feulner, R. Kienberger, and J. Burgdörfer, Real-time observation of collective excitations in photoemission, Phys. Rev. B **91**, 241101(R) (2015).

[9] J. Riemensberger, S. Neppl, D. Potamianos, M. Schäffer, M. Schnitzenbaumer, M. Ossiander, C. Schröder, A. Guggenmos, U. Kleineberg, D. Menzel, F. Allegretti, J. V. Barth, R. Kienberger, P. Feulner, A. G. Borisov, P. M. Echenique, and A. K. Kazansky, Attosecond Dynamics of *sp*-Band Photoexcitation, Phys. Rev. Lett. **123**, 176801 (2019).

[10] R. O. Kuzian and E. E. Krasovskii, One-step theory of photoelectron escape time: Attosecond spectroscopy of Mg(0001), Phys. Rev. B **102**, 115116 (2020).

[11] J. D. Lee, Final-state effects on delayed photoemission in the attosecond streaking of core level spectral lines of copper dihalides, Phys. Rev. B **86**, 035101 (2012).

[12] J. D. Lee, Model for the Attosecond Resonant Photoemission of Copper Dichloride: Evidence for High-Order Fano Resonances

and a Time-Domain Core-Hole Clock, Phys. Rev. Lett. **111**, 027401 (2013).

[13] M. Drescher, M. Hentschel, R. Kienberger, M. Uiberacker, V. Yakovlev, A. Scrinzi, Th. Westerwalbesloh, U. Kleineberg, U. Heinzmann, and F. Krausz, Time-resolved atomic inner-shell spectroscopy, Nature **419**, 803 (2002).

[14] R. Kienberger, E. Goulielmakis, M. Uiberacker, A. Baltuska, V. Yakovlev, F. Bammer, A. Scrinzi, T. Westerwalbesloh, U. Kleineberg, U. Heinzmann, M. Drescher, and F. Krausz, Atomic transient recorder, Nature **427**, 817 (2004).

[15] M. Uiberacker, Th. Uphues, M. Schultze, A. J. Verhoef, V. Yakovlev, M. F. Kling, J. Rauschenberger, N. M. Kabachnik, H. Schröder, M. Lezius, K. L. Kompa, H.-G. Muller, M. J. J. Vrakking, S. Hendel, U. Kleineberg, U. Heinzmann, M. Drescher, and F. Krausz, Attosecond real-time observation of electron tunnelling in atoms, Nature **446**, 627 (2007).

[16] E. Goulielmakis, Z.-H. Loh, A. Wirth, R. Santra, N. Rohringer, V. S. Yakovlev, S. Zherebtsov, T. Pfeifer, A. M. Azzeer, M. F. Kling, S. R. Leone, and F. Krausz, Real-time observation of valence electron motion, Nature **466**, 739 (2010).

[17] S. Biswas, B. Förg, L. Ortmann, J. Schötz, W. Schweinberger, T. Zimmermann, L. Pi, D. Baykusheva, H. A. Masood, I. Liontos, A. M. Kamal, N. G. Kling, A. F. Alharbi, M. Alharbi, A. M. Azzeer, G. Hartmann, H. J. Wörner, A. S. Landsman, and M. F. Kling, Probing molecular environment through photoemission delays, Nat. Phys. **16**, 778 (2020).

[18] I. Jordan, M. Huppert, D. Rattenbacher, M. Peper, D. Jelovina, C. Perry, A. von Conta, A. Schild, and H. J. Wörner, Attosecond spectroscopy of liquid water, Science **369**, 974 (2020).

[19] R. Pazourek, J. Feist, S. Nagele, and J. Burgdörfer, Attosecond Streaking of Correlated Two-Electron Transitions in Helium, Phys. Rev. Lett. **108**, 163001 (2012).

[20] A. K. Kazansky and P. M. Echenique, One-Electron Model for the Electronic Response of Metal Surfaces to Subfemtosecond Photoexcitation, Phys. Rev. Lett. **102**, 177401 (2009).

[21] L. Hedin, J. Michiels, and J. Inglesfield, Transition from the adiabatic to the sudden limit in core-electron photoemission, Phys. Rev. B **58**, 15565 (1998).

[22] L. Hedin and J. D. Lee, External losses in photoemission from strongly correlated quasi-two-dimensional solids, Phys. Rev. B **64**, 115109 (2001).

[23] D. C. Langreth, Singularities in the x-ray spectra of metals, Phys. Rev. B **1**, 471 (1970).

[24] B. Gumhalter, V. Kovač, F. Caruso, H. Lambert, and F. Giustino, On the combined use of GW approximation and cumulant expansion in the calculations of quasiparticle spectra: The paradigm of Si valence bands, Phys. Rev. B **94**, 035103 (2016).

[25] J.-J. Chang and D. C. Langreth, Deep-hole excitations in solids. II. Plasmons and surface effects in x-ray photoemission, Phys. Rev. B **8**, 4638 (1973).

[26] J. S. Zhou, J. J. Kas, L. Sponza, I. Reshetnyak, M. Guzzo, C. Giorgetti, M. Gatti, F. Sottile, J. J. Rehr, and L. Reining, Dynamical effects in electron spectroscopy, J. Chem. Phys. **143**, 184109 (2015).

[27] J. C. Ashley and R. H. Ritchie, Quantum treatment of multiple real transitions, Phys. Rev. **174**, 1572 (1968).

[28] S. Hüfner, *Photoelectron Spectroscopy* (Springer-Verlag, Berlin, Heidelberg, New York, 2003).

[29] J. M. Dahlström, A. L'Huillier, and A. Maquet, Introduction to attosecond delays in photoionization, J. Phys. B: At., Mol. Opt. Phys. **45**, 183001 (2012).

[30] A poor screening of the photohole is signified by the difference in the plasmon vacuum states between without and with core hole, i.e., $|0'\rangle \neq |0\rangle$ in Eq. (2).